Korean J. Chem. Eng., 39(7), 1717-1728 (2022)
DOI: 10.1007/s11814-022-1066-7

pISSN: 0256-1115
eISSN: 1975-7220

Numerical study of fly ash deposition process in low temperature economizer under SCR conditions

Shuangcheng Fu*,, Gang Cao*,**, Guofu Ou*,**, Faqi Zhou*,**,†, and Luyu Li*,****

*School of Mechanical Engineering, Changzhou University, Changzhou 213164, China
**Jiangsu Key Laboratory of Green Process Equipment, Changzhou 213164, Jiangsu, China
(*Received 24 September 2021 • Revised 7 January 2022 • Accepted 13 January 2022*)

Abstract−After the boiler of a thermal power plant in Nanjing was reformed for denitrification, the clogging of fly ash particles occurred near the support beam of the economizer. The critical speed criterion under different working conditions was constructed by Fluent custom code (UDF), and the change of fly ash deposition on the support beam of the economizer was simulated without ABS and with ABS. At the same time, the influence of the fin layout structure on the movement of smoke and fly ash particles was analyzed. The results show that the stagnation of fly ash particles on the supporting beam is the main cause of sediment clogging. Due to the production of ABS in the process of denitrification, the adhesion of fly ash particles is intensified. At the same time, the fin structure on the support beam hinders the lateral movement of fly ash particles, which causes the growth of clogged fly ash near the support plate. On this basis, an optimization plan for the fin structure is proposed, which improves the flue gas flow conditions and avoids the occurrence of clogging and growth of fly ash.

Keywords: SCR, Particle Deposition, Particle Collision, Critical Velocity, Numerical Simulation

INTRODUCTION

In the coal-fired boilers of thermal power plants, it is common that the deposition of fly ash particles causes boiler blockage. Fly ash deposition on the wall will reduce the heat transfer efficiency of the heating surface, which can reduce the heat transfer efficiency of the boiler by 10% [1]. After the selective catalytic reduction (SCR) denitrification technology is adopted by the boiler, ammonia often escapes in the denitrification reactor. The SO_3 in the equipment reacts with the escaped ammonia to produce ammonium bisulfate (ABS) and ammonium sulfate (AS), and the sulfate as a binder promotes the growth of deposits [2,3]. At the same time, the accumulation of fly ash particles in the economizer will cause the problems of flue gas bypass and local increase in flow velocity, which will lead to erosion and wear and affect the safe operation of equipment.

Many scholars have conducted simulation studies on the transport and deposition of fly ash particles. Inertial impact, thermophoresis, and turbulent diffusion are the deposition mechanisms by which fly ash particles are deposited on the wall [4-6]. For the deposition behavior of monodisperse particles, fly ash particles with smaller particle sizes are mainly determined by turbulent diffusion. Inertial collision is the main deposition mechanism of larger fly ash particles [7]. Lin et al. [8] found that the deposition of fly ash particles is greatly affected by the particle size, and it also plays an important role in the distribution of deposition on the wall of the tube bundle. At the same time, the flow rate and pressure drop are affected by the roughness of the pipeline, which increases the deposition rate of small particles in the tube bundle [9]. Mu et al. [10] studied the deposition and formation of fly ash, and analyzed the influence of different parameters (such as particle diameter, flow rate, and temperature) on the deposition of fly ash on different tube rows. Wang et al. [11] simulated the structural characteristics of the finned tube and analyzed their influence on deposition by optimizing the number of rows, tube spacing, and other structural parameters.

According to the latest research progress, various fly ash deposition models have been developed to better predict the behavior of fly ash deposition [12]. The deposition of fly ash on the wall is mostly judged based on viscosity [13,14] and speed. However, compared with the speed deposition judgment model, the disadvantage of the viscous deposition model is that these models cannot be used to study the influence of parameters such as velocity and angle. For this reason, a velocity-based fly ash deposition mechanics model has been proposed and perfected. If the incident velocity of the particles is less than the critical velocity, they will be deposited on the wall, otherwise they will rebound. Generally, there is always dust accumulation on the tube bundle, so the dust accumulation layer should be regarded as a solid surface. The critical velocity and normal recovery coefficient are used to describe the deposition behavior of the particles. Han et al. [15] studied the particle deposition characteristics on a heat exchanger tube by the deposition model, and analyzed the influence of particle diameter, flow velocity, and tube number arrangement on the deposition. Konstandopoulos [16] gave a new criterion for the oblique critical impact angle. When the incident angle of particles is greater than the critical angle, fly ash particles will not deposit even if the incident velocity is less than the critical adhesion velocity. At the same time, the adhered particles may rebound due to the effect of the smoke near the wall. Therefore, EI-Batsh et al. [17] developed a particle deposition model

†To whom correspondence should be addressed.
E-mail: zhoufaqi@cczu.edu.cn

based on the critical velocity of particles, including adhesion, bouncing, and peeling processes. Ahmadi [18] theoretically analyzed the deposition and removal mechanisms of particles in turbulent flow, and combined them with the critical moment theory to evaluate the removal conditions of particles of different sizes. Pan et al. [19] accurately predicted the growth of fouling on the economizer tube bundle, taking into account the standards of particle deposition, rebound, and removal. But in the denitrification equipment, the strong viscosity between fly ash particles is the main cause of fly ash growth. For the ABS deposition area, we studied the macroscopic deposition characteristics of fly ash particles in the economizer on the basis of the elastic collision deposition of loose fly ash, while considering the viscous effect.

This paper takes the denitrification retrofit boiler of a thermal power plant in Nanjing as the research object, and establishes the speed criterion for the loose ash accumulation on the economizer support beam and the ABS adhesion ash accumulation. A fly ash deposition model was constructed by using Fluent custom function (UDF), and the ash accumulation process was studied numerically based on the field measured data of a thermal power plant. By changing the fin layout structure on the supporting beam, the influence of different structures on the deposition amount was analyzed, which provides guidance for the industrial design of the economizer.

NUMERICAL METHODS

1. Continuum Phase Governing Equations

Flue gas flow is a three-dimensional unsteady incompressible flow. Considering the flow and heat transfer between the flue gas and the finned tube, the governing equations in the calculation domain are as follows.

Continuity equation:

$$\frac{\partial \rho u_i}{\partial x_i} = 0 \tag{1}$$

Momentum equation:

$$\frac{\partial (u_i u_k)}{\partial x_i} = \frac{\partial}{\partial x_i}\left(v\frac{\partial u_k}{\partial x_i}\right) - \frac{1}{\rho}\frac{\partial p}{\partial x_k} \tag{2}$$

Energy equation:

$$\frac{\partial (\rho u_i T)}{\partial x_i} = \frac{\partial}{\partial x_i}\left(\frac{\lambda}{c_p}\frac{\partial T}{\partial x_i}\right) \tag{3}$$

where x_i is the tensor coordinate, u_i is the average velocity component in the x_i direction, m/s; ρ is the flue gas density, kg/m^3; p is the pressure, Pa; c_p is the specific heat capacity of the flue gas at constant pressure, J/(kg·K); λ is the thermal conductivity, W/(m·K); T is the flue gas temperature, K.

In this paper, the flow velocity of the flue gas is 4-8 m/s. The numerical simulation uses the RNG k-ε turbulence model to describe the turbulence motion of the flue gas. The RNG k-ε turbulence model was developed on the basis of the standard k-ε turbulence model. It has higher accuracy and better reliability. Therefore, the RNG k-ε turbulence model [20] was used to study the effect of turbulence on the flow.

The RNG k-ε turbulence model is as follows:

$$\rho\frac{Dk}{Dt} = \frac{\partial}{\partial x_i}\left(\alpha_k \mu_{eff}\frac{\partial k}{\partial x_i}\right) + \mu_t S^2 - \rho\varepsilon \tag{4}$$

$$\rho\frac{D\varepsilon}{Dt} = \frac{\partial}{\partial x_i}\left(\alpha_\varepsilon \mu_{eff}\frac{\partial \varepsilon}{\partial x_i}\right) + C_{1\varepsilon}\frac{\varepsilon}{k}\mu_t S^2 - C_{2\varepsilon}\rho\frac{\varepsilon^2}{k} - R_\varepsilon \tag{5}$$

$$R_\varepsilon = \frac{C_\mu \rho \phi^3 (1-\phi/\phi_0)}{1+\beta\phi^3}\frac{\varepsilon^2}{k} \tag{6}$$

In the formula, $\mu_{eff}=\mu+\mu_t$ and $\mu_t=\rho C_\mu k^2/\varepsilon$ with C_μ=0.0845, Φ=sk/ε, Φ_0=4.38, β=0.012, $C_{1\varepsilon}$=1.42 and $C_{2\varepsilon}$=1.68, α_k and α_ε are the inverse effective Prandtl numbers for k and ε, $\alpha_k=\alpha_\varepsilon$=1.393 are used in the simulation.

2. Discrete Phase Model

The Lagrangian calculation method is used to calculate the motion of the discrete phase. For the movement of particles, due to the low particle concentration in the flue gas, the volume rate of particles is less than 10%. The DPM model is used to track the trajectory of each particle. The control equation of the particle is:

$$\frac{dU_p}{dt} = F_D(U-U_p) + \frac{g(\rho_p-\rho)}{\rho_p} + F_A \tag{7}$$

In the formula, U and U_p represent the velocity of the gas phase and the particle phase, respectively; ρ and ρ_p represent the density of the gas phase and the particle phase, respectively; G is the acceleration of gravity; t represents the time; $F_D(U-U_p)$ is the resistance acting on the particles. $F_D=18\mu C_D Re_p/(24\rho_p d_p^2)$, C_D is the drag coefficient; F_A is the additional force, that is, the thermophoretic force received by the particles. Due to the large particle size of fly ash herein, the effect of thermophoretic force can be ignored [21].

3. Mechanical Deposition Model

For the sedimentation characteristics of fly ash particles in the tube bundle, the traditional research is that the fly ash deposits when it contacts the tube wall [22]. However, to improve the sedimentation accuracy of fly ash particles, it is also necessary to consider the rebound characteristics of fly ash particles [23,24]. Through the UDF model, an equation for the critical velocity of fly ash deposition is established. In the model calculation, only the elastic effect of the loose accumulation of ash is considered, and the viscous effect is ignored. However, for ABS viscous fouling, the combined effect of viscosity and elasticity is considered. By setting parameters such as wall Young's modulus and Poisson's ratio [25], two critical fouling criteria at different speeds were established. Therefore, the model can simultaneously simulate the loose accumulation of ash and the ABS-attached ash. The critical velocity equation proposed by Brach and Dunn [26] is as follows:

$$u_{cr} = \left(\frac{2E}{d_p}\right)^{\frac{10}{7}} \tag{8}$$

In the formula, d_p is the particle size of fly ash, E is Young's modulus of the composite material, and the formula for calculating Young's modulus of the composite material is:

$$E = 0.51\left[\frac{5\pi^2(k_1+k_2)}{4\rho_p^{1.5}}\right]^{0.4} \tag{9}$$

In the formula,

$$k_1 = \frac{1-\nu_m^2}{\pi E_m} \tag{10}$$

$$k_2 = \frac{1-\nu_p^2}{\pi E_p} \tag{11}$$

where ν_m and ν_p are the Poisson ratios of the wall and fly ash particles, respectively. E_m and E_p are Young's modulus of the wall and fly ash particles.

Under the scour of flue gas and the collision of other particles, the deposited particles may still be separated. When the friction velocity of the wall fluid is greater than the critical shear velocity, the particles will be separated. The calculation formula for the critical shear rate u_{π} is:

$$u_{\pi c}^2 = \frac{W_A}{\rho d_p}\left(\frac{3W_A}{4d_p E}\right)^{1/3} \tag{12}$$

In the formula, W_A is the adhesion constant, which is 0.039 J/m^2.

4. Simulation Process

To describe the deposition state of loose and sticky fly ash particles, the movement of fly ash particles is constrained by the loaded UDF. When the normal speed of fly ash particles is less than the critical speed, they will deposit on the wall, otherwise they will rebound. When the friction velocity of the fluid on the wall surface is greater than the critical shear velocity, the particles will be separated. In the simulation process, particle trajectory tracking is used to determine whether fly ash particles are deposited on the support beam wall. The numerical simulation process of fly ash particle sedimentation is shown in Fig. 1.

CASE DESCRIPTION AND SOLUTION STRATEGY

1. Engineering Case

With increasing attention to environmental protection issues, reducing NO_x emissions through denitrification is imperative. The SCR reactor and boiler flue of a thermal power plant in Nanjing are shown in Fig. 2(a). An SCR reactor is added between the high-temperature economizer and the high-temperature preheater, and the purpose of denitrification is achieved by injecting ammonia gas to react with NO_x. In the low-temperature economizer running the denitrification process, the presence of liquid ABS increases the adhesion of fly ash particles. It can be seen from Fig. 2(b), (c) that the dust accumulation on both sides of the support plate above the support beam is serious, and the dust accumulation area under the support plate is larger than the dust accumulation area above the support plate. It is preliminarily judged that the ash accumulation gradually accumulates from below the support plate upwards, and the start of the ash accumulation is on the beam directly below the support plate.

2. Physical Model and Meshing

A simplified model was carried out based on the tube bundle size of the economizer. The tube bundle is simplified into a row of seven heat exchange tubes, and a schematic diagram of the structure is shown in Fig. 3. The H-shaped finned tubes in the economizer are arranged in parallel, and the grid is shown in Fig. 3(c). Because the entrance and exit parts of the model are relatively regular, in order to save memory and have higher precision, a structured grid is adopted. For the H-shaped fin area in the middle of the economizer, an adaptable unstructured grid is adopted, and the grid at the tube bundle is encrypted. Since the grid near the wall

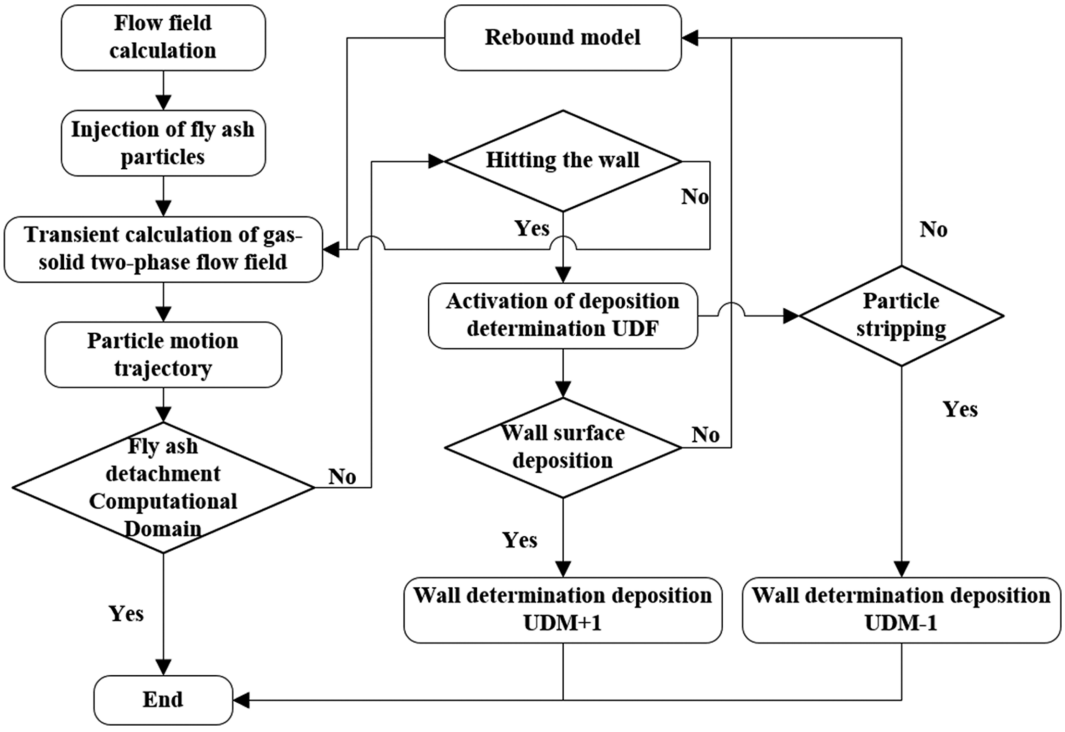

Fig. 1. Numerical simulation of fly ash deposition process.

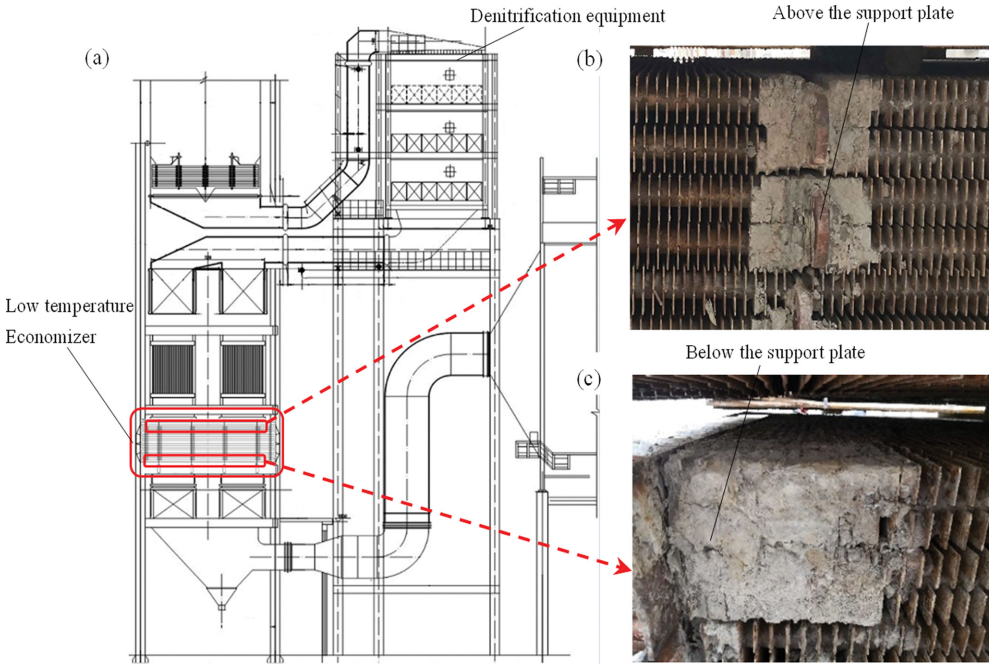

Fig. 2. Site plan of boiler system and blockage (a) schematic diagram of boiler reactor and flue, (b) block diagram above the support plate, (c) blockage diagram under the support plate.

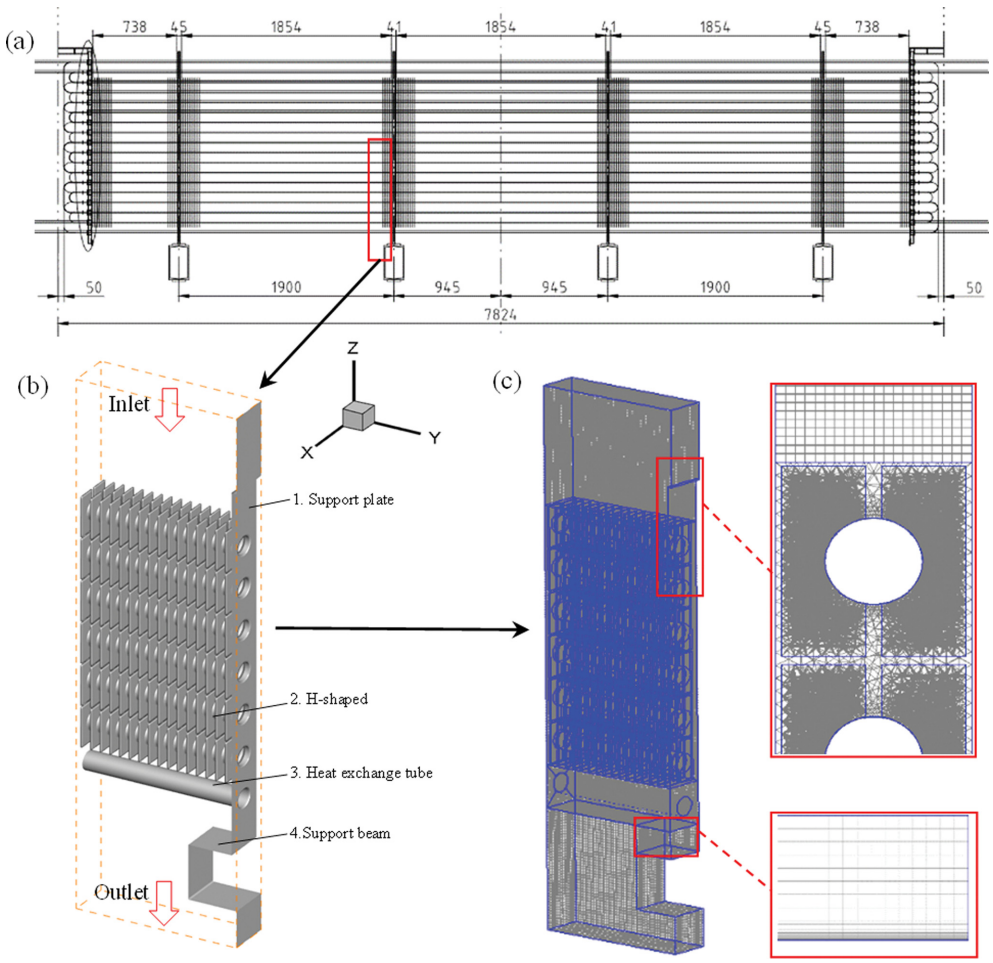

Fig. 3. Schematic diagram of economizer structure (a) geometry schematic, (b) simplified structure diagram, (c) three-dimensional grid.

Table 1. Average Nu number under different grid numbers

Number of grids	481,350	743,096	1,506,202	2,701,241	3,607,340
Average Nu number	123.68	108.7	94.4	90.83	87.6

Table 2. Physical properties of deposition model

Parameter	Values	Parameter	Values
Dynamic viscosity of flue gas (Pa·s)	3.328×10^{-5}	Flue gas density (kg/m^3)	0.67
Particle flow of soot (kg/s)	0.001	Inlet velocity of flue gas (m/s)	4
Inlet temperature of flue gas (K)	548	Temperature of the pipe wall (K)	513
Young's modulus of ABS ash accumulation section (Pa)	4×10^5	Young's modulus of soot particles (Pa)	9×10^{10}
Restoration coefficient of ABS cohesive fouling area [28]	0.4	Restoration coefficient of loose fouling area [28]	0.9
Poisson's ratio of soot particles	0.27	Poisson's ratio of the support beam	0.31

of the beam has a greater impact on the boundary layer, the grid near the wall is encrypted to ensure that the grid size of the first layer is $y^+\approx1$. In the numerical simulation of fly ash deposition, the number of grids increased from 481,350 to 3,607,340, and the corresponding simulated Nu number is shown in Table 1. When the number of grids further increases and the Nu value changes by less than 5%, the grids are considered to meet the independent requirements [27]. Considering the accuracy and economy of the simulation, a model with a grid number of 1,506,202 is selected for numerical calculation.

3. Solution

The simulation work was performed in the transient mode in Fluent 18.0. The pressure-based solver was adopted, and the pressure-velocity coupling was completed through the SIMPLE scheme. The convergence criterion is that the normalized residual of each governing equation is less than 1.0×10^{-4}. The DPM model was used to simulate the movement of fly ash particles in the calculation area, and the number of deposited particles increases with time. In the same time interval, the number of fly ash particles deposited can be calculated, and then the deposition rate can be calculated. The relevant parameters in the simulation are shown in Table 2.

4. Model Validation

Since the movement of fly ash particles on the convective heating surface is closely related to the density and velocity distribution of the flue gas, it is of great significance to accurately predict the fluid flow and heat transfer characteristics near the heating surface. To verify the accuracy of the numerical simulation results, the numerical simulation results were compared with the Žukauskas empirical related equations. The related equations of Žukauskas [29] are as follows:

$$Nu_f = cRe^m Pr^n \left(\frac{Pr}{Pr_w}\right)^{0.25} \tag{13}$$

$$\Delta p = f\times\frac{1}{2}\rho U_{max}^2 z \tag{14}$$

where U_{max} is the maximum velocity of the flue gas at the smallest cross-section in the calculation domain, f is the friction coefficient, and z is the number of pipe rows. The Reynolds number Re is between 12,223 and 24,445, and the corresponding flue gas velocity range is 4 to 8 m/s. In the correlation equation, the constant term c=0.27, m=0.63, n=0.36.

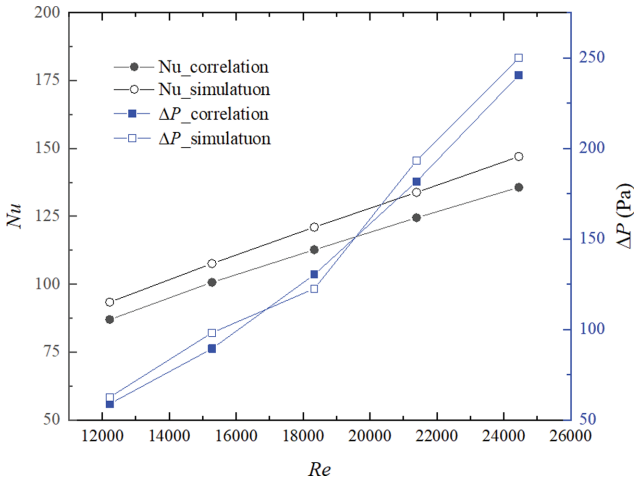

Fig. 4. Nu and ΔP comparison between the simulations and experimental correlations.

The Nu and pressure drop values were compared with the corresponding experimental values as shown in Fig. 4. It can be seen that the experimental and simulated values conform to the law and trend, and the maximum deviations of Nu and pressure drop from the experimental values are 9% and 10%, respectively. The Reynolds number studied in this paper is 12,223, and the errors of the corresponding Nu and pressure drop values are both less than 7%, which further illustrates the accuracy of the simulation.

SIMULATION RESULTS AND ANALYSIS

1. Flue Gas Field and Particle Trajectory

The flue gas flow state in the YZ plane at the center of the economizer tube bundle is shown in Fig. 5. The velocity cloud picture, turbulent kinetic energy distribution, and streamline distribution are shown in Fig. 5. The velocity of the flue gas inlet is 4 m/s, and the flue gas flows around due to the existence of the supporting beam. The flue gas flow rate above the supporting beam is very low, as shown in Fig. 5(a). The turbulent kinetic energy distribution

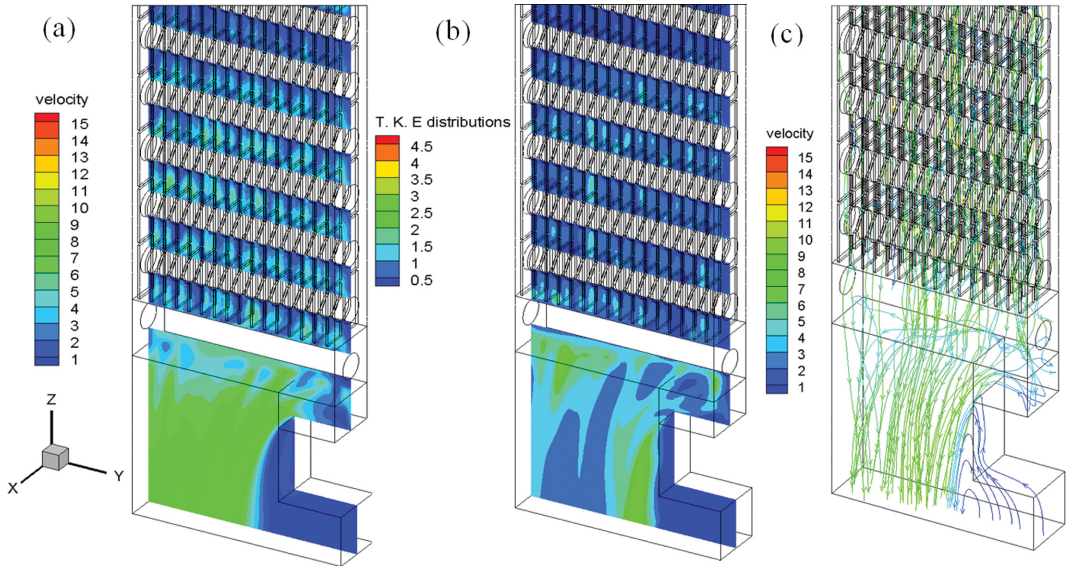

Fig. 5. YZ plane flow field in the center of the economizer (a) velocity cloud, (b) turbulent kinetic energy distribution, (c) streamline distribution.

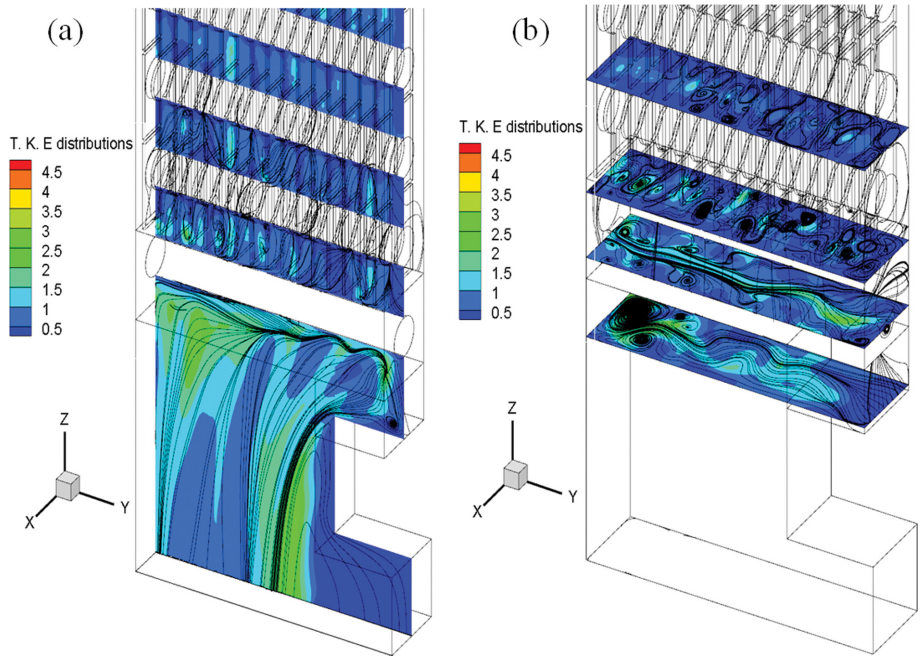

Fig. 6. Turbulent structure and secondary flow (a) YZ plane flow structure, (b) XY plane secondary flow field.

in the YZ plane is shown in Fig. 5(b). The turbulence energy on the upper surface of the support beam is significantly smaller than the turbulence energy around the support beam. This may cause fly ash particles with a smaller particle size to change their direction of movement through turbulent dispersion. The streamline of the YZ plane is shown in Fig. 5(c), and the color indicates the flow rate of the flue gas. We found that there are backflow and vortex phenomena of flue gas on the support beam, and these vortex phenomena are very important for the particle deposition on the support beam.

To better observe the flue gas flow near the support beam of the economizer and the secondary flow of flue gas on the upper surface of the support beam, the enlarged turbulent structure and secondary flow are shown in Fig. 6. Fig. 6(a) shows the flow structure of the flue gas. As the flow of flue gas is hindered by the tube bundles and fins, there are stagnant vortices between the tube bundles. At the same time, with the flue gas flowing around on the supporting beam, there is an obvious low-speed smoke stagnation area on the supporting beam. For fly ash particles with a smaller particle size, the flue gas turbulence and stagnant vortices have strong entrainment and trapping effects. Fig. 6(b) shows the secondary flow field in the channel. It can be seen from the figure that the secondary

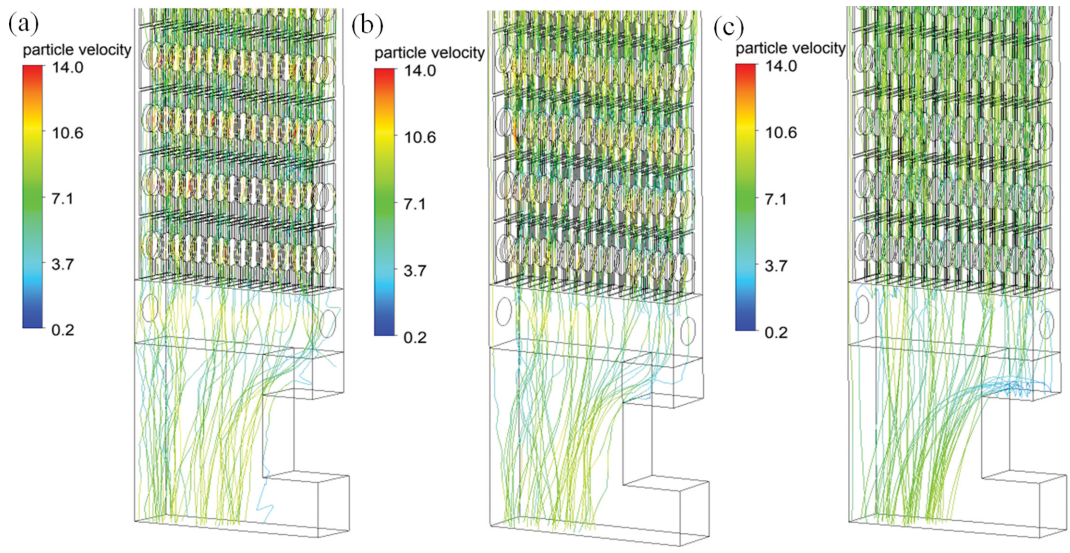

Fig. 7. Effect of particle size on flow trajectory(a) d_p=1 μm, (b) d_p=10 μm, (c) d_p=50 μm.

flow in the XY plane between the first two fins is relatively obvious, and secondary flow in the last XY plane above the beam basically does not exist. The results show that the presence of fins has a more significant effect on the flue gas flow, and the tube bundle is mainly affected by the vertical stagnation vortex.

The three-dimensional trajectory diagrams of different particles are shown in Fig. 7, and the particle sizes in the figure are 1 μm, 10 μm, and 50 μm, respectively. The color in Fig. 7 indicates the velocity of fly ash particles. It can be found that the velocity of fly ash particles on the upper surface of the support beam is relatively low. For fly ash particles with d_p=1 μm, it can be found that the trajectories of the particles above the supporting beam cross each other and are prone to moving around the beam. As shown in Fig. 7(a), the collision with the upper wall of the support beam is less. This is because the flow structure of flue gas tends to change the trajectory of small particles, and the direction of motion is affected by the dispersion of turbulence. However, in Fig. 7(c), for fly ash particles with d_p=50 μm, due to the large inertia of the particles, the particle flow around the support beam is significantly reduced. At the same time, the number of particles hitting the upper surface of the support beam increased. This is because gravity settlement and inertial impact gradually dominate, and it is easy to get rid of the flow following effect of flue gas. Therefore, fly ash particles of different particle sizes have different deposition mechanisms, and fly ash particles with larger particle sizes are more likely to deposit on the upper wall of the support beam.

2. Influence of Particle Size on Deposition Characteristics

The deposition efficiency of fly ash particles on the support beam is shown in Fig. 8, and the flue gas flow rate is 4 m/s. It can be seen from Fig. 8 that as the particle size increases, the deposition efficiency on the upper wall of the support beam continues to increase. For fly ash particles with d_p<10 μm, the deposition rate of fly ash on the support beam is low, and the gravity sedimentation is not obvious. As shown in the previous section, this is because small particles are susceptible to flue gas flow and move around the beam. The deposition behavior is mainly turbulence and Brownian diffusion. For particles with 10 μm<d_p<50 μm, the deposition rate of fly ash particles on the support beam is significantly increased. This is because the combination of turbulent diffusion and inertial shock enhances the particle deposition ability, and the inertial shock gradually dominates. When the fly ash particle size d_p>50 μm, the deposition rate on the support beam gradually tends to be flat, reaching a relatively constant value. Because inertial impact has become the major mechanism of deposition as particle size rises, the deposition process tends to be steady. Through fly ash sampling and analysis, it is concluded that the average particle size of fly ash particles deposited in the economizer is 84 μm, which further indicates that loose fly ash deposits are prone to appearing on the support beams.

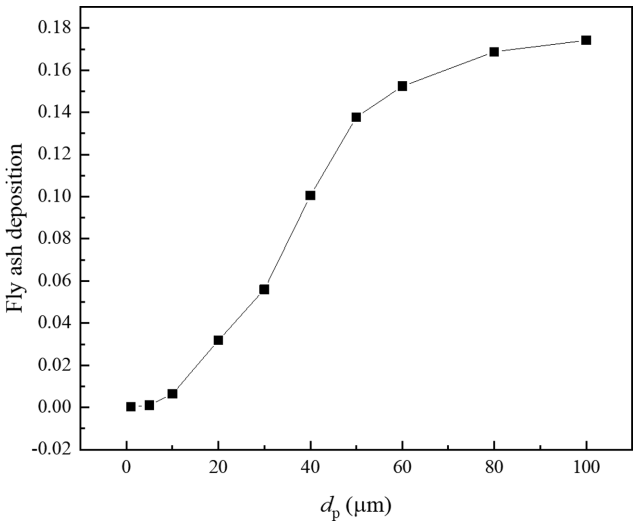

Fig. 8. Effect of particle size on deposition efficiency.

The 3D deposition of fly ash particles on the support beam of the economizer is shown in Fig. 9, which more significantly shows the deposition dynamics of fly ash particles at d_p=1 μm, 10 μm,

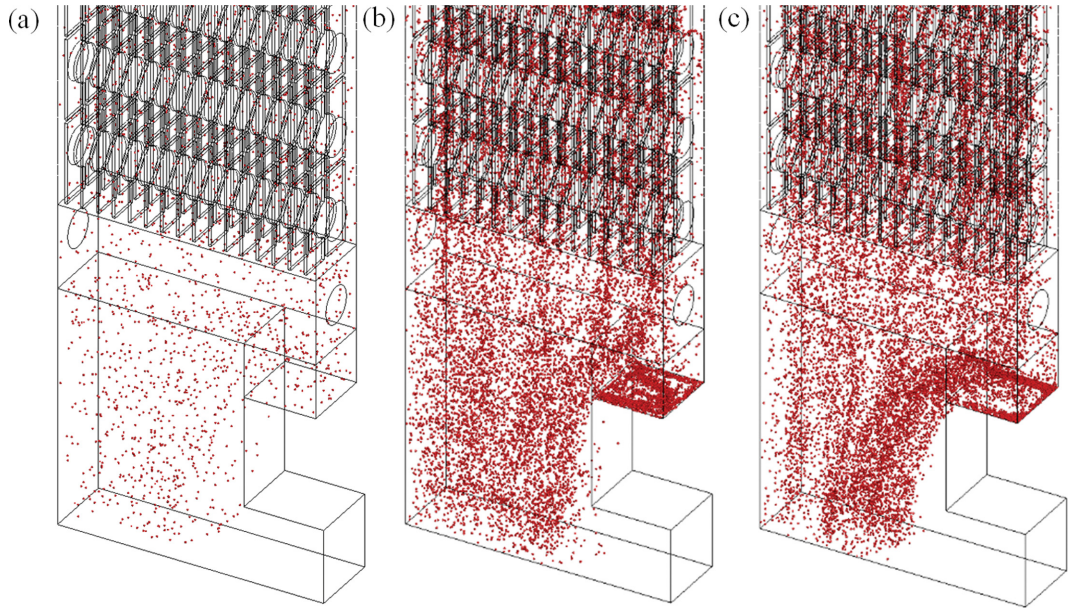

Fig. 9. Effect of particle size on deposition characteristics on support beams. (a) d_p=1 μm (b) d_p=10 μm (c) d_p=50 μm.

and 50 μm. The number of fly ash particles deposited between the support beam and the fins is lower when d_p=1 μm. As discussed in the section on flue gas flow field and particle trajectory, this is because the smaller fly ash particles have greater followability and the influence of the flue gas flow on the fly ash particles is more significant. Because of the high inertia, it is relatively difficult to change the trajectory when the particle size is 10 μm or 50 μm, and it is easy to be intercepted by the windward side. In contrast to the deposition dynamics of small particles, more particles can be found between the fins and the upper surface of the support beam. Therefore, it can be concluded that as particle size increases, gravity sedimentation gradually becomes the dominant factor in particle deposition. In addition, due to the collision of particles with the windward wall, the number of deposited particles on the upper wall of the support beam increases significantly.

3. The Influence of ABS on Deposition Characteristics

ABS reactants are produced during the process of denitrification, and the melting temperature of ABS is 420-553 K. It is in a molten state around 473-513 K and has strong viscosity. According to on-site temperature detection, the working temperature of the flue gas near the supporting beam below the low-temperature economizer is about 503 K, which is located in this area. Therefore, loose fouling without ABS will be transformed into cohesive fouling with ABS, and its growth ability will be enhanced, which will accelerate the deposition rate of fly ash.

The mass distribution of loose ash deposition without ABS and viscous ash deposition with ABS for fly ash particles with d_p=84 μm is shown in Fig. 10. As seen, the amount of cohesive fly ash deposited between the fins and on the support beam is substantially more than the amount of loose fly ash. Because the liquid ABS is attached to the support beam, Young's modulus of the support beam wall is reduced, and the critical speed of fly ash particle deposition is increased, resulting in a significant amount of fly ash particle deposition in this location. From the growth trend of cohesive fly ash deposition in Fig. 10, it can be seen that the outer side of the upper wall of the support beam is the initial deposition site, and the fly ash deposition grows from the outer side of the upper wall to the inner side of the support plate. This is because the movement of the fly ash particles is affected by the effect of the flue gas around the support beam, so the trajectory of the fly ash movement will deviate to the outside. At the same time, the presence of the fins above the supporting beam restricts the lateral flow of fly ash particles between the fins, which in turn leads to easy deposition on the beam. As the amount of deposition continues to increase, the fly ash on the beam will also accumulate and grow to the inside.

The change curve of fly ash deposition on the support beam is shown in Fig. 11. The deposition quality curve under different working conditions in the figure shows that the deposition quality of fly ash with ABS is greater under denitrification working conditions. The deposition quality of fly ash with ABS is more than seven times that of fly ash without ABS. As the operating time of the equipment increases, the gap in the amount of deposition further expands. It further proved the correctness of the theoretical hypothesis and verified the clogging phenomenon of fly ash in the field equipment (Fig. 2). Due to the special arrangement structure of the H-shaped fins, the upper surface of the support beam is continuously accumulated and grown by fly ash particles under the action of ABS.

4. Structure Optimization

In a previous simulation, the deposition properties of fly ash particles on the support beam were studied, and it was determined that the presence of fins hinders the lateral flow of fly ash particles. At the same time, the ABS produced by the denitrification process enhances fly ash particle adhesion, causing blockage near the support plate. In this section, a plan for optimizing the equipment structure is proposed, starting with the idea of reducing the deposition of fly ash particles on the support beam. For the solution to reduce the deposition of fly ash on the support beam, the idea is to opti-

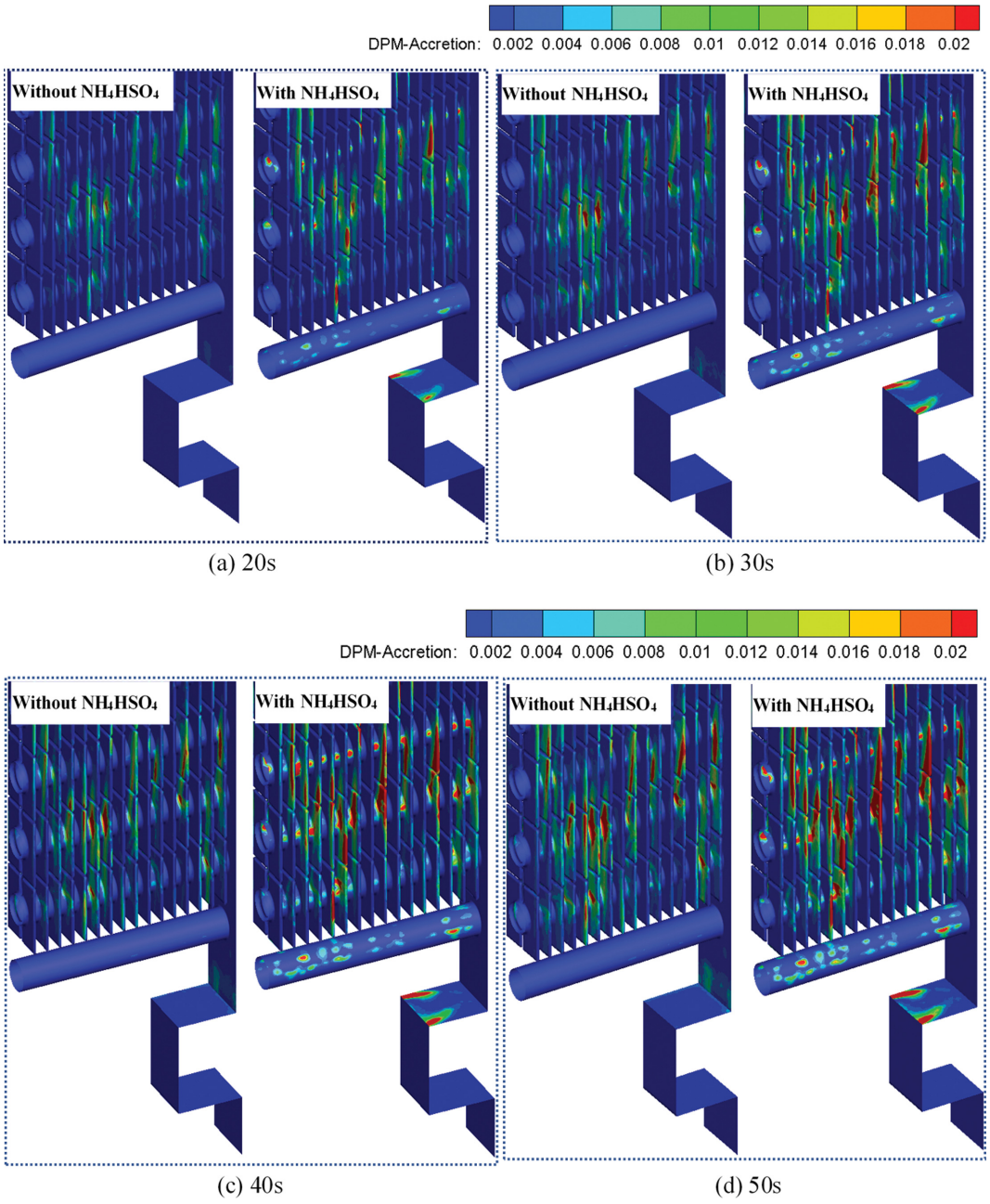

Fig. 10. Deposition mass clouds at different moments.

mize the flue gas flow field and fly ash particle trajectory by changing the arrangement of the fins above the support beam. The size of the structure is shown in Fig. 12, and a new fin arrangement structure is proposed. A pyramid-shaped area is divided above the supporting beam, and no H-shaped fins are provided in this area.

The turbulent energy distribution of the optimized and original structures is shown in Fig. 13. As can be observed, the turbulence energy above the optimized structural support beam has increased. As previously stated, the flow trajectory of fly ash particles with smaller particle sizes is easily affected by the turbulent dispersion of flue gas. After the structure is optimized, the turbulent kinetic energy above the support beam is significantly higher than that of the original structure, which is conducive to the deposition of small particles.

In Fig. 14, the deposition rate of fly ash particles with different particle sizes is shown. It can be seen that when d_p<30 μm, the deposition rate of fly ash particles on the optimized structure is greater than that of the original structure. This is because fly ash particles of small particle size are affected by turbulent dispersion, which increases the probability of collision with the wall. When d_p>30 μm, the deposition rate of fly ash particles on the optimized structure is significantly lower than that of the original structure. This is because fly ash particles of larger particle sizes are easy to get rid of the effect of flue gas flow, reducing the influence of turbulent flue gas dispersion on the support beam. Simultaneously, the removal of the fins above the support beams enhances the lat-

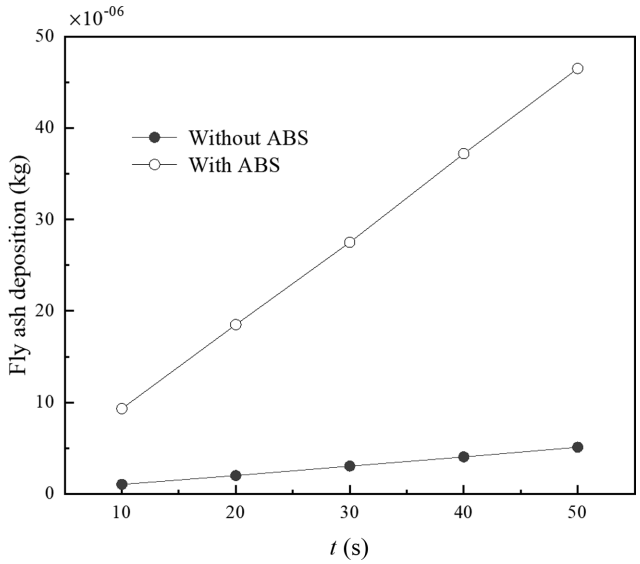

Fig. 11. Deposited mass of fly ash particles on beams.

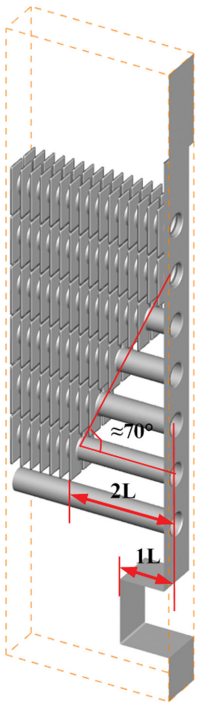

Fig. 12. Optimized structure.

eral movement ability of fly ash particles, resulting in a reduction in deposition rate. Compared with the average particle size of the fly ash clogged by field equipment, it further shows that structural optimization is beneficial for reducing the fly ash clogging on the support beam.

We changed the arrangement of the fins above the support beam, which inevitably led to complex changes in the heat transfer performance and resistance characteristics of the economizer. The Nu number and Eu number were compared with the Re as shown in Fig. 15. As seen there, the Nu number of the new structure is smaller than that of the original structure under the same Re conditions. This is because optimizing the fin structure reduces the heat transfer area, resulting in a reduction in heat transfer performance. At the same time, the reduction of fins leads to an increase in the flue gas flow area, and the drag coefficient of the economizer is reduced to a certain extent. The Re number in this study is 12,223, and Nu and Eu are reduced by 4.8% and 4.4%, respectively, both within the acceptable range. In addition, since the simulation is based on the simplification of the economizer structure, the calculation domain is much smaller than the actual structure size. Therefore, the

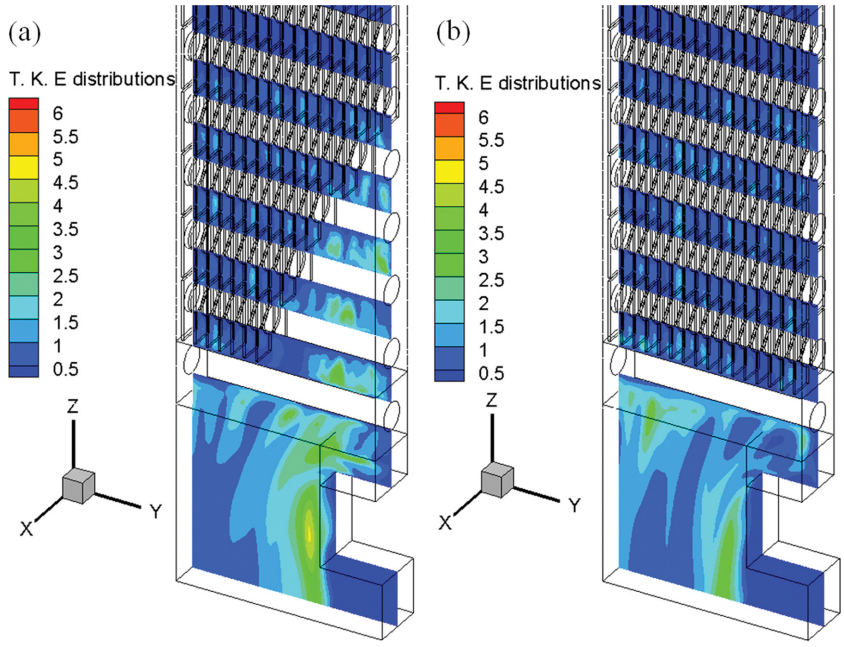

Fig. 13. Turbulent energy diagram (a) optimized structure, (b) original structure.

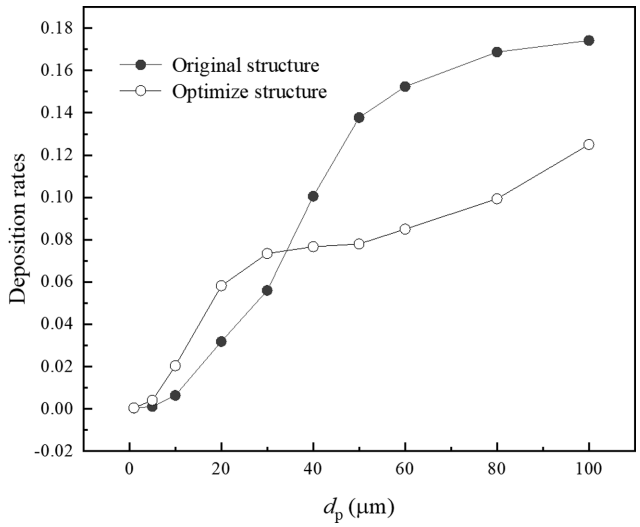

Fig. 14. Deposition rates of different particle sizes on different structures.

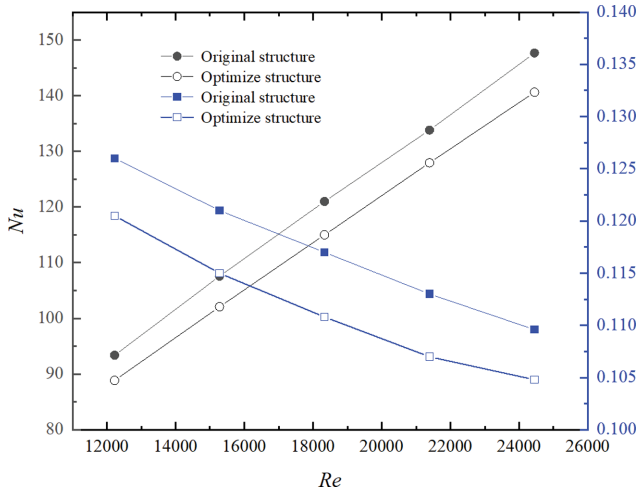

Fig. 15. Nu and Eu numbers: comparison between original and optimized structure.

Nu and Eu errors of different structures should be further reduced, so that the influence of structural changes on the heat transfer performance of the economizer can be ignored.

The simulation results show that ABS has a greater impact on the fly ash deposition on the support beam, and the quality of fly ash deposition increases with the increase of the particle size. Under denitrification conditions, the physical condensation of ABS on the support beam and the low-speed flow of flue gas caused the fly ash near the support plate to block. By optimizing the arrangement of the fins above the supporting beam, the deposition of fly ash particles on the supporting beam can be effectively reduced, which provides a reference for the structural design and transformation of the low-temperature economizer.

CONCLUSION

The macroscopic properties of fly ash particles deposited in the economizer are discussed in this paper. Using the computational fluid dynamics method, the flue gas field near the supporting beam and fins was obtained. The influence of the flue gas field on the deposition of fly ash on the support beam is discussed, and a structural improvement plan to reduce the amount of dust accumulation on the beam is proposed. The main conclusions are as follows:

(1) The flue gas flow characteristics of the economizer were obtained through numerical simulation, and the low-speed flow of flue gas on the supporting beam is the main reason for the deposition of fly ash particles.

(2) The ABS produced in the denitrification process changes the properties of fly ash and accelerates the deposition rate of fly ash particles. The deposition quality of the ABS bonding area and the loose ash deposit area were compared and analyzed, and it was found that the deposition quality of the ABS bonding area is more than seven times that of the loose ash deposit area.

(3) The fin structure above the support beam is optimized, which effectively improves the lateral flow of smoke. The collision rate of fly ash particles on the upper wall of the support beam is greatly reduced, thereby avoiding the growth of fly ash clogging along the fins.

ACKNOWLEDGEMENTS

This work was supported by Postgraduate Research & Practice Innovation Program of Jiangsu Province (Grant No. KYCX21_2811), Natural Science Research Project of Jiangsu Higher Education Institutions (Grant No. 20KJA470001).

NOMENCLATURE

u_{cr}	: critical deposition rate [m/s]
E	: composite Young's modulus [N/m^2]
E_p	: Young's modulus of particles [N/m^2]
E_m	: Young's modulus of the deposited surface [N/m^2]
T_{in}	: inlet temperature [K]
T_w	: tube wall temperature [K]
Pr	: Prandtl Number
Pr_w	: Wall Prandtl Number
F_D	: drag force [N]
F_A	: additional power [N]
d_p	: particle diameter [mm]
ν_m	: deposited surface poisson ratio
ν_p	: particle poisson's ratio
z	: number of tube rows
U	: gas phase velocity [m/s]
U_p	: particle phase velocity [m/s]
C_D	: resistance factor
Re_p	: particle phase Reynolds number
Re	: gas phase Reynolds number

Greek Symbols

v	: power viscosity [m^2/s]
ρ_p	: particle phase density [kg/m^3]
ρ	: gas phase density [kg/m^3]
f	: coefficient of friction

REFERENCES

1. C. J. Tsai, J. S. Lin, S. G. Aggarwal and D. R Chen, *Aerosol Sci. Tech*., **38**, 131 (2004).
2. Y. Shi, H. Shu, Y. Zhang, H. Fan, Y. Zhang and L. Yang, *Fuel Process. Technol*., **150**, 141 (2016).
3. Y. Wang, H. Tan, K. Dong, H. Liu, J. Xiao and J. Zhang, *Appl. Therm. Eng*., **118**, 283 (2017).
4. B. E. Lee, C. A. J. Fletcher, S. H. Shin and S. B. Kwon, *Fuel*, **81**, 2001 (2002).
5. Z. Zheng, W. Yang, H. Wang, A. Zhou, Y. Cai, G. Zeng and H. Xu, *Energy*, **220**, 119699 (2021).
6. H. Han, Y. He, W. Tao and Y. Li, *Int. J. Heat Mass Tran*., **72**, 210 (2014).
7. H. Lu, L. Lu and Y. Jiang, *Appl. Therm. Eng*., **110**, 150 (2017).
8. L. Mu, L. Zhao and H. Yin, *Appl. Therm. Eng*., **44**, 57 (2012).
9. W. Hong and X. Wang, *Korean J. Chem. Eng*., **35**, 1517 (2018).
10. L. Mu, S. Wang, Z. Zhai, Y. Shang, C. Zhao, L. Zhao and H. Yin, *J. Energy Inst*., **93**, 1481 (2020).
11. F. Wang, Y. He, S. Tang and Z. Tong, *Int. J. Heat Mass Tran*., **112**, 367 (2017).
12. Y. Cai, K. Tay, Z. Zheng, W. Yang, H. Wang, G. Zeng, Z. Li, S. K. Boon and P. Subbaiah, *Appl. Energ*., **230**, 1447 (2018).
13. M. Walsh Peter, N. Sayre Alan, O. Loehden David, S. Monroe Larry, M. Beér János and F. Sarofim Adel, *Prog. Energy Combust. Sci*., **16**, 327 (1990).
14. A. Brink, D. Lindberg, M. Hupa, M. E. de Tejada, M. Paneru and J. Maier, *Fuel Process. Technol*., **141**, 210 (2016).
15. H. Han, Y. He, W. Tao and Y. Li, *Int. J. Heat Mass Tran*., **72**, 210 (2014).
16. A. G. Konstandopoulos, *J. Aerosol Sci*., **37**, 292 (2006).
17. H. El-Batsh and H. Haselbacher, *ASME Paper*. GT-2002-30600 (2002).
18. C. Toscano and G. Ahmadi, *J. Adhesion*, **79**, 175 (2010).
19. Y. Pan, F. Si, Z. Xu and C. E. Romero, *Powder Technol*., **210**, 150 (2011).
20. F. Wang, Y. He, Z. Tong and S. Tang, *Int. J. Heat Mass Tran*., **104**, 774 (2017).
21. S. Tang, F. Wang, Q Ren and Y. He, *Fuel*, **203**, 725 (2017).
22. Z. Zhang and Q. Chen, *Atmos. Environ*., **43**, 319 (2008).
23. K. Sun, *Indoor Built Environ*., **20**, 300 (2011).
24. H. Jiang, L. Lu and K. Sun, *Build. Environ*., **45**, 1184 (2009).
25. M. Luo, L. Zhao and S. Li, *J. Chin. Soc. Power Eng*., **36**, 883 (2016).
26. R. M Brach and P. F. Dunn, *Aerosol Sci. Tech*., **16**, 51 (1992).
27. F. Wang, Y. He, S. Tang and Z. Tong. *Chinese Sci. Bull*., **62**, 1292 (2017).
28. R. Israel and D. E. Rosner, *Aerosol Sci. Tech*., **2**, 45 (1982).
29. A. A. Žukauskas and R. V. Ulinskas, *Heat Tran. Eng*., **6**, 19 (1985).